

Article

Implications of Major and Trace Element Migration in Altered Granites for Hydrothermal Alteration and Granite-Related Uranium Mineralization in the Sanjiu Ore Field, South China

Xu Chen ^{1,2,3,4,*}, Chunhua Wen ³, Debao Meng ³, Bin Li ³, Biguang Jiang ² and Jinning Qin ²¹ School of Geosciences and Info-Physics, Central South University, Changsha 410083, China² Geological Bureau of Hunan Province, No. 306 Brigade, Hengyang 421000, China; hnsdzyjbg@126.com (B.J.); hn306dk@163.com (J.Q.)³ Geological Survey of Hunan Institute, Changsha 410116, China; herowch2004@163.com (C.W.); mengdebao2003@163.com (D.M.); cuglibin@163.com (B.L.)⁴ Cooperative R&D Center of Postdoctoral Programme, Geological Survey of Hunan Institute, Changsha 410116, China

* Correspondence: sugar-19851007@163.com; Tel.: +86-182-1600-6242

Abstract: The recently discovered Sanjiu ore field (SJOF) is a granite-related uranium ore field located in the middle of Zhuguangshan (South China). The relationship between hydrothermal alteration of granite and uranium mineralization in the SJOF is crucial yet understudied. In this study, the major- and trace-element contents of granite samples (fresh granite, altered granite, and tectonites) with different uranium contents were analyzed by using X-ray fluorescence spectroscopy (XRF) and inductively coupled plasma–mass spectrometry (ICP–MS). The analytical results show a relative increase in Si, S, Ca, Pb, Mo, and Sb content in altered granites and tectonites, relative to fresh granites. During the mineralization stage, the increase of the aforementioned elements is related to various hydrothermal alterations (e.g., silicification, carbonation, sulfation, etc.) and newly formed minerals (e.g., microfine crystalline quartz veins; calcite agglomerates or fine veins; and metal sulfides, such as pyrite). There is a concomitant relative decrease in Na, K, Al, Fe, Mg, and other elemental contents that may be due to mineralogical alteration processes, such as biotite to chlorite, feldspar-group minerals to clay minerals, and redox of Fe-bearing minerals. The LREE/HREE ratio in altered granites decreases significantly with the increase in uranium content, suggesting that a low LREE/HREE ratio may be a prospecting indicator. The normalized trace-element patterns of mineralized granite (ore) and the relatively high U content of fresh granite imply that granitic rocks may be the primary uranium source in the SJOF. The uranium mineralization is mainly concentrated in the redox zone that occurs at a depth of 100–300 m. The redox zone is characterized by the most developed hydrothermal alterations and enrichment of trace elements, including W, Mo, Sb, Li, and the HREE.

Keywords: granite-related uranium deposit; major and trace elements; uranium mineralization; Sanjiu ore field; Zhuguangshan



Citation: Chen, X.; Wen, C.; Meng, D.; Li, B.; Jiang, B.; Qin, J. Implications of Major and Trace Element Migration in Altered Granites for Hydrothermal Alteration and Granite-Related Uranium Mineralization in the Sanjiu Ore Field, South China. *Minerals* **2022**, *12*, 144. <https://doi.org/10.3390/min12020144>

Academic Editor: David Quirt

Received: 21 December 2021

Accepted: 21 January 2022

Published: 25 January 2022

Publisher's Note: MDPI stays neutral with regard to jurisdictional claims in published maps and institutional affiliations.



Copyright: © 2022 by the authors. Licensee MDPI, Basel, Switzerland. This article is an open access article distributed under the terms and conditions of the Creative Commons Attribution (CC BY) license (<https://creativecommons.org/licenses/by/4.0/>).

1. Introduction

The uranium (U) deposits in China are generally hosted by four types of rocks: granites, volcanic rocks, carbonaceous–siliceous–pelitic rocks, and sandstones. The granite-related U deposits comprise about 35% of the U reserves in China [1]. The Zhuguangshan composite granitic batholith (ZCGB) is an important U host in South China, as it is associated with most of the identified granitic U resources. The Sanjiu ore field (SJOF) is located in Zhuguangshan between the Lujing ore field and the Chengkou ore field in the middle of the ZCGB (Figure 1).

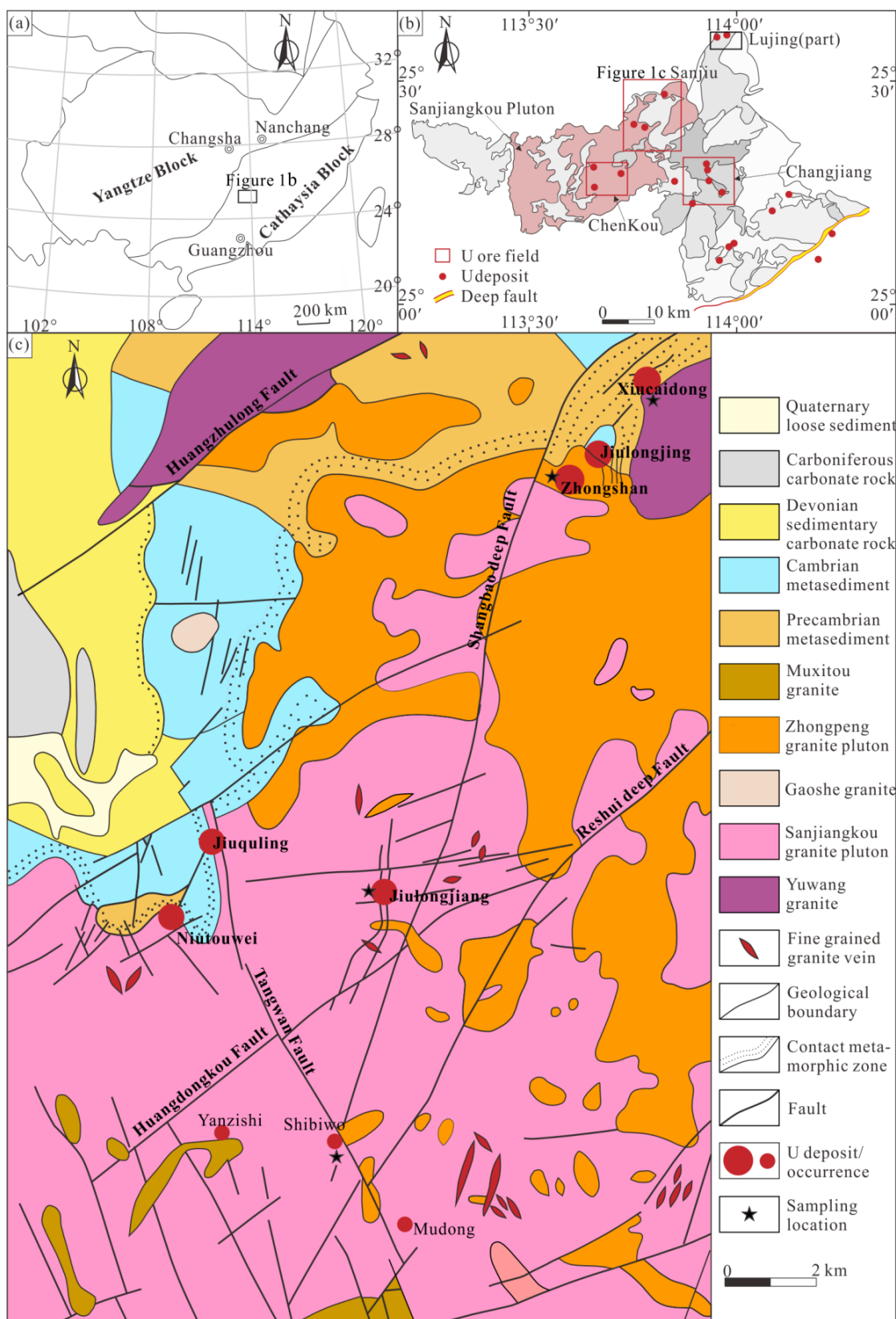


Figure 1. (a) Geotectonic location map of the ZCGB. (b) Schematic map of granitic plutons and U ore fields in central and southern part of the ZCGB. (c) Simplified geological map of the SJOF. Notes: Figure 1a modified from Mao et al. [2], Figure 1b modified from Deng et al. [3], and Figure 1c modified from Chen et al. [4].

It is a recent discovery, within the last twenty years, of granite-related U mineralization. The metallogenic characteristics of the SJOF, such as tectonic setting, strata, petrology, structure, orebody, and ore genesis, have been previously well documented (see References [4–15], and the references therein). These previous studies have demonstrated that the granitoids from the Late Jurassic are the main host-rocks and the main U source for these medium-to-low temperature hydrothermal deposits in the SJOF. They have shown that the hosts for the U in the granites are mainly uraninite and coffinite, and, to a lesser extent, monazite and apatite. Trace amounts of uraninite are found as inclusions in biotite, so biotite only indirectly sources a small amount of U. Medium–low temperature hydrothermal alteration styles (e.g., silicification, hematitization, pyritization, chloritization, hydromica, and fluorination) of the host-rock are described in References [1,4–15]. Previous studies have focused on the geochronology and geochemistry of the fresh granites (FG) [9,10] and found that granite hosting U mineralization has a high U content; more than three times the average U content (3.5–4.8 ppm) of typical acidic igneous rocks [13,14]. These granites are generally characterized by genesis through crustal partial melting, high-silica, high-alkali, and peraluminous character [9–11,16,17]. It is believed that the prerequisites for the U mineralizing potential of these U-rich granites lie not only in the high U content, but also in the development of active faults and fluid-flow-related hydrothermal alterations. However, the characteristics of element migration within altered granites in terms of U mineralization and hydrothermal alteration remain unclear.

Hydrothermal mineralization is a complex geological process in which mineralizing elements and other active elements in geological bodies are released, exchanged, transported, and enriched to form the mineralization at the structural and/or chemical trap [18]. The hydrothermal reactions and the characteristics of the mineralization environment are closely linked to element migration. Studying the changes of major and trace elements in geological bodies helps to understand the mineralization process and characteristics [19,20]. This paper presents petrographic observations and whole-rock geochemical analyses of altered granites and tectonites (strongly altered granites) associated with U mineralization. This work aims to compare the element migration in various altered granites with different U contents and provide valuable information for research and exploration of the SJOF.

2. Regional Geology and Deposit Geology

The middle section of the ZCGB is located in the east part of the famous Nanling metallogenic belt of the Cathaysian block. It is a U-prospective area that contains multiple uplift zones, deep faults, and other favorable fluid-flow conditions. Many granite-related U ore fields, such as Sanjiu, Lujing, Chengkou, and Changjiang, have been discovered in and around the ZCGB (Figure 1b) [21–23].

The SJOF is named after the granite-related U deposits discovered in and around the Jiulongjing, Jiuquling, and Jiulongjiang mining areas. It covers an area of approximately 120 km² and is located at the junction of the Guangdong, Hunan, and Jiangxi provinces (Figure 1b). The outcropping strata are mainly exposed in the northwest of SJOF. The Precambrian and Cambrian strata comprise mainly U-rich low-grade weakly metamorphosed marine sedimentary rock. The Devonian strata are composed of clastic sedimentary rocks and shallow-water carbonates. The Carboniferous strata are mainly shallow-water carbonate. Finally, the Quaternary strata are composed of mainly loose diluvium and sediments. The magmatic rocks of the SJOF are mainly Jurassic granite. The largest granite bodies are the Sanjiangkou and Zhongpeng plutons, which are also U-rich and U-producing. The Sanjiangkou pluton is mainly medium-to-coarse-grained biotite monzogranite with an emplacement age of 161.9 ± 2.1 Ma [6,7]). The Zhongpeng pluton is mainly fine-grained two-mica granite with an emplacement age of 148.2 ± 1.9 Ma [6]. In addition to these plutons, there are some Late Cretaceous granites and fine-grained granite dykes that do not show uranium mineralization. The Jurassic granites are highly fractionated peraluminous S-type granites derived from partial melting of U-rich metasediments [9,10,24]. The main rock-controlling fault in the SJOF is the NE-trending Shangbao-Reshui deep fault, whereas

the mineralization-controlling faults are generally NE-, NNE-, and NW-trending secondary faults (Figure 1c).

As with most granite-related U deposits in South China, the mineralization age (100–45 Ma) of those deposits in the SJOF is significantly younger than the age (162–148 Ma) of granite plutonism [9–11]. U mineralization is usually associated with dark-red and variegated siliceous veins, dark-red microcrystalline quartz, smoky quartz, variegated chalcedony, dark-purple fluorite, granite breccia, cataclastic-altered granite, etc. U mineralization in the deposits is generally hosted in the deformed part of fault, the interface between fault and Jurassic pluton, and in the interlayer fracture zone. Mineralization typically occurs as vein, lens, and stockwork configurations in the mineralization-controlling faults with dimensions ranging from 50 to 150 m in length, 0.7 to 15 m in width, and 50 to 350 m in depth. Mineralization is generally of siliceous vein, breccia, and cataclastic altered-rock types. Host-rock hydrothermal alteration closely related to mineralization mainly includes hematitization, pyritization, silicification, dark-purple fluoritization, clay alteration, etc. The principal U minerals are pitchblende and uraninite, as well as small amounts of coffinite, uranothorite, etc. [11–13]. The mineral paragenesis has been divided into three stages in the SJOF [4].

3. Materials and Methods

3.1. Sampling

Thirty granite samples were collected from deep boreholes or outcrops in the Zhongshan, Jiulongjiang, and Xiucaidong granite-related U deposits, and the newly found Shibiwo occurrence (Figure 1 and Table 1). These samples comprise fresh granites (no obvious alteration), altered granites, and tectonites. The altered granites and tectonites are classified into three categories according to their U content: barren samples ('BS', U content < 0.01%), mineralized samples ('MS', U content ranging from 0.01% to 0.05%), and mineralized (ore-bearing) samples ('OBS', U content > 0.05%). The specific properties and locations of the samples are shown in Table 1 and Figure 2. The fresh granites collected from the Sanjiangkou pluton are characterized by a gray-white or light pink color, and both porphyritic and massive textures. They are mainly composed of K-feldspar (25%–35%), plagioclase (25%–30%), quartz (30%–35%), and biotite (3%–5%) (Figure 2a). The hydrothermal alteration of the granite presents disseminated or veinlet hematitization, pyritization, chloritization, dark-purple fluoritization, dark-red or variegated microcrystalline quartz vein, carbonation dominated by calcite, kaolinization, and other clay mineral alterations (Figure 2). From fresh granite to altered granite and/or tectonite, the mineralogical characteristics are presented as follows: (1) more anhedral mineral habits rather than euhedral and subhedral mineral habits, (2) a significant increase in the amount of altered minerals with metasomatic residual structure, and (3) more developed microcracks in minerals.

Table 1. Geological characteristics and location of the SJOF granite samples.

Sample No.	Lithology	Type	Sample Location	Mining Area
ZS07	Altered granite	BS	ZKZ4, burial depth 315 m	Zhongshan
ZS09	Cataclastic-altered granite	BS	ZKZ1, burial depth 163 m	
SBW13	Fresh biotite monzogranite	FG	ZK10, burial depth 80 m	Shibiwo
SBW24	Cataclastic-altered granite	BS	Outcrop, burial depth 0 m	
SBW26	Cataclastic-altered granite	BS	ZK01, burial depth 126 m	
SBW28	Cataclastic-chloritized rock	BS	ZK72, burial depth 161 m	

Table 1. Cont.

Sample No.	Lithology	Type	Sample Location	Mining Area
JLJ02	Cataclastic-altered granite	MS	ZK71, burial depth 125 m	Jiulongjiang
JLJ03	Cataclastic-altered granite	MS	ZK71, burial depth 198 m	
JLJ04	Altered granite	MS	ZK63, burial depth 265 m	
JLJ07	Cataclastic-altered granite	OBS	ZK39, burial depth 100 m	
JLJ08	Cataclastic-altered granite	OBS	ZK16, burial depth 196 m	
JLJ09	Fresh biotite monzogranite	FG	ZK16, burial depth 184 m	
JLJ10	Cataclastic-altered granite	OBS	ZK39, burial depth 99 m	
JLJ11	Cataclastic-altered granite	OBS	ZK71, burial depth 130 m	
JLJ13	Cataclastic-altered granite	OBS	ZK71, burial depth 135 m	
JLJ17	Cataclastic-altered granite	OBS	ZK02, burial depth 119 m	
JLJ24	Cataclastic-altered granite	MS	ZK95, burial depth 311 m	
JLJ26	Fresh biotite monzogranite	FG	ZK87, burial depth 234 m	
JLJ27	Cataclastic-altered granite	OBS	ZK73, burial depth 237 m	
JLJ28	Cataclastic-altered granite	OBS	ZK16, burial depth 195 m	
JLJ29	Weakly altered granite	BS	ZK95, burial depth 384 m	
JLJ30	Cataclastic-altered granite	MS	ZK79, burial depth 246 m	
JLJ31	Cataclastic-altered granite	MS	ZK63, burial depth 171 m	
JLJ33	Cataclastic-altered granite	OBS	ZK47, burial depth 539 m	
XCD02	Cataclastic-altered granite	BS	ZK55, burial depth 309 m	Xiucaidong
XCD07	Cataclastic-altered granite	BS	ZK63, burial depth 66 m	
XCD09	Cataclastic-altered granite	MS	ZKX2, burial depth 473 m	
XCD12	Altered granite	BS	ZK47, burial depth 60 m	
XCD13	Kaolinized cataclastic rock	BS	ZK44, burial depth 315 m	
XCD15	Cataclastic-altered granite	MS	Outcrop, burial depth 0 m	

Note: Most of the cataclastic altered granites that do not display granite texture are tectonites.

3.2. Whole-Rock Geochemistry

Whole-rock major- and trace-element contents of the samples were obtained through analyses carried out at the ALS Laboratory Group, Mineral Division–ALS Chemex (Guangzhou, China), by using inductively coupled plasma mass spectrometry (ICP–MS, model Agilent 7700X, Agilent Technologies, Santa Clara, CA, USA) and X-ray fluorescence spectrometry (XRF, model PANalytical PW2424, Malvern Panalytical, Eindhoven, The Netherlands). The samples were first milled to about 200 mesh in a contamination-free agate mill and were split into two subsamples. One subsample was fused with lithium borate/lithium nitrate and then analyzed for major element oxide contents by XRF (relative deviation < 5%, relative error < 2%). The other subsample was digested through alkali fusion and four-acid digestion, and then analyzed for trace element contents by using ICP–MS (relative deviation < 10%, relative error < 10%). The detailed testing processes are described by the national standards Methods for Chemical Analysis of Silicate Rocks (GB/T 14506.14–2010) [25] and Chemical Reagent-General Rules for Inductively Coupled Plasma Mass Spectrometry (GB/T 39486–2020) [26].

3.3. Mass Balance Considerations Related to Host-Rock Alteration

Consideration of mass-balance calculations of chemical-element mobility (gains and losses) from fresh granite to altered granite to mineralized granite was carried out. The key to the mass-balance calculation is the selection of a stable inactive (immobile) component. Many studies have used Al₂O₃ or some other geochemical element that did not participate in the strong alteration [27,28]. However, due to the large collection area for the sampling and the many types of host-rock alterations present in the samples, the selection of a suitable immobile component is difficult. For example, the Al₂O₃ contents of altered granites vary greatly; Figure 3b). In our previous exploration work, it was found that (1) the densities of fresh granites in the SJOF are 2.65–2.70 g/cm³, while the densities of various altered granites (including MS and OBS) are 2.62–2.68 g/cm³; and (2) the volume change between fresh granite and altered granite is also very small (generally <3.07%), even after releasing

a large amount of uranium. Based on this premise, more detailed mass balance calculations (such as those described by References [29,30]) were not carried out. The error in the calculated absolute changes of chemical elements in altered granite is not more than 3.05%, which is far less than the content change of major elements, and, thus, the influence on the content change of trace elements can be ignored.

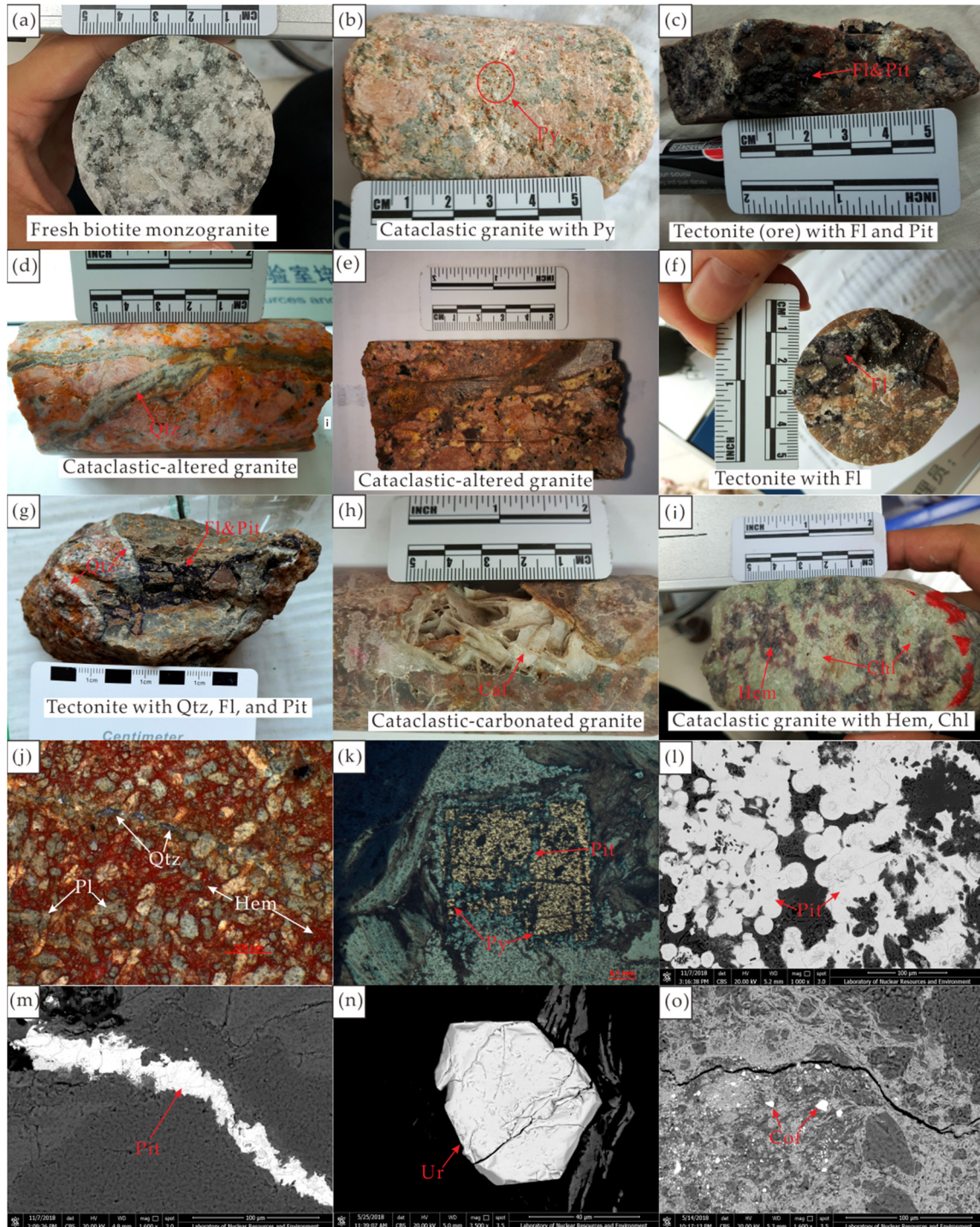


Figure 2. Representative samples and minerals from the SJOF. Notes: Images (a–i) are hand specimen photographs; images (j,k) are optical micrographs; images (l–o) are backscatter micrographs. Abbreviations: Pit—pitchblende; Qtz—Quartz; Py—pyrite; Hem—hematite; Fl—fluorite; Pl—plagioclase; Cal—calcite; Chl—chlorite; Ur—uraninite; Cof—coffinite.

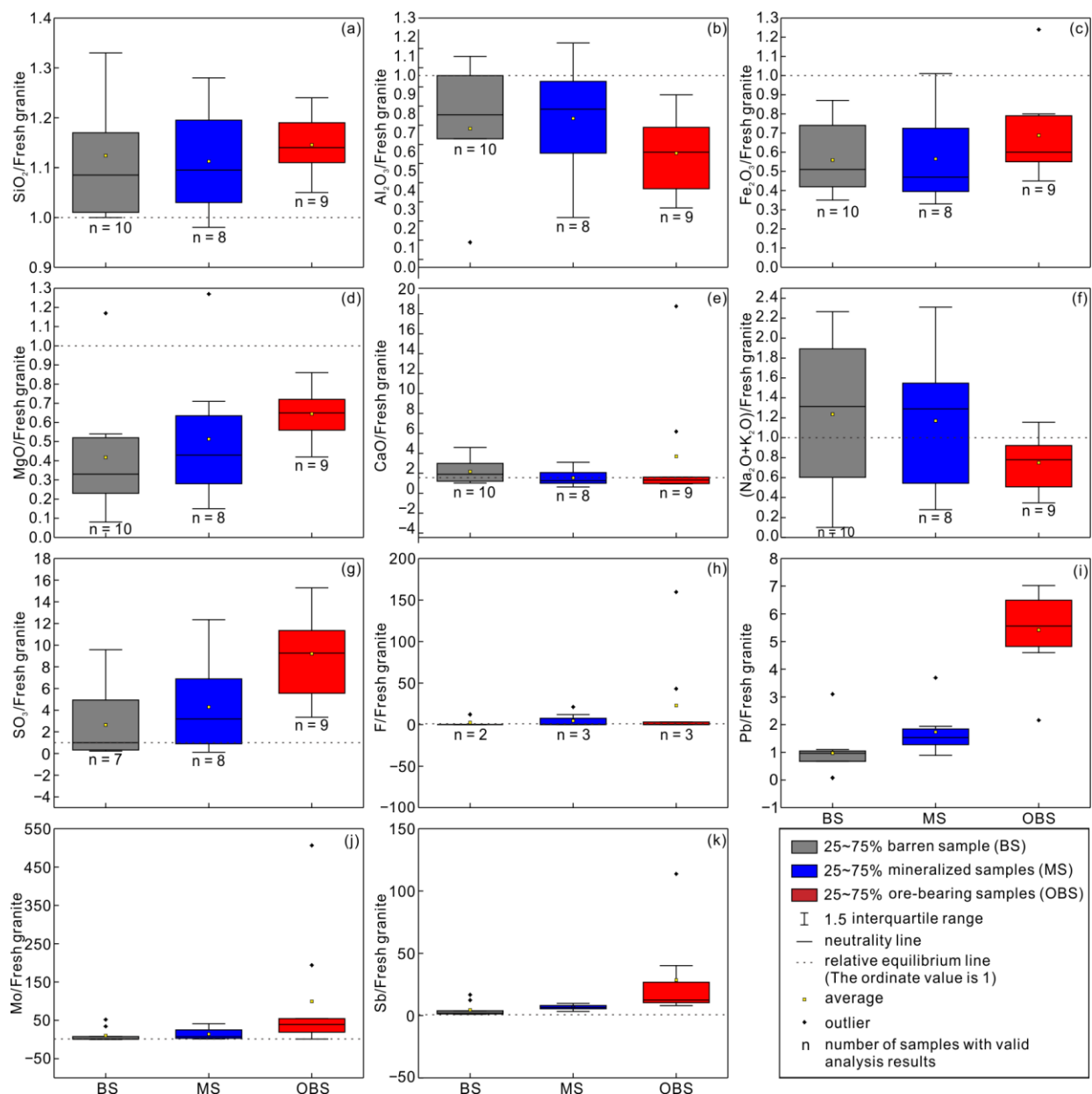


Figure 3. Box-whisker diagrams showing relative contents of important elements, namely Pb, Mo, and Sb, in altered SJOF granites. (a) SiO_2 , (b) Al_2O_3 , (c) Fe_2O_3 , (d) MgO , (e) CaO , (f) $\text{Na}_2\text{O} + \text{K}_2\text{O}$, (g) SO_3 , (h) F , (i) Pb , (j) Mo , (k) Sb .

The major and trace elements of fresh granite in the SJOF were selected as the base values for simple and intuitive geochemical normalization calculations and comparisons. Using these normalized values, the relative migration of major and trace elements during alteration of fresh granite to altered granite can be deduced, and the calculation of absolute mass balance changes is not necessary to the data interpretation, discussion and conclusions in this study.

4. Results

4.1. Major Element Contents

Whole-rock geochemical analyses for major elements are presented in Table 2 and Appendix A Table A1. The results show that the major element and U composition of fresh granites are quite different from that of altered granites and tectonites. Compared with the fresh granites, the altered granites and tectonites have more

variable geochemical compositions, with higher SiO₂ (69.97–94.47 wt%, average 80.12 wt%), CaO (0.03–8.32 wt%, average 0.90 wt%), SO₃ (Bld–1.32 wt%, average 0.45 wt%), F (Bld–5.10 wt%, average 0.32 wt%), and U (4.12–1154 ppm, average 402.38 ppm) contents and lower Al₂O₃ (1.84–16.86 wt%, average 10.06 wt%), Fe₂O₃(total) (TFe₂O₃; 0.82–3.09 wt%, average 1.50 wt%), MgO (0.04–0.66 wt%, average 0.27 wt%), Na₂O (0.03–4.02 wt%, average 0.99 wt%), and K₂O (0.41–6.86 wt%, average 4.08 wt%) contents. The average loss on ignition (LOI) of altered granite and tectonite (1.53 wt%) is higher than that of fresh granite (1.09 wt%), indicating that the former has experienced hydrothermal alteration and/or weathering. Figure 3a–h shows fresh granites-normalized (Appendix A) major element contents of the altered granites and tectonites with different uranium contents. As shown in the box-whisker diagram in Figure 3, most of the average major-element contents of the altered granite and tectonite mostly have a relatively consistent change trend in parallel with the increase in U content. These change trends correspond to one or more hydrothermal alteration features of the host-rock.

Table 2. Geochemical summary of major-element oxides (wt%) and U (ppm) of SJOF granite samples.

	SiO ₂	Al ₂ O ₃	Fe ₂ O _{3T}	MgO	CaO	Na ₂ O	K ₂ O	SO ₃	F	U	LOI
	Fresh granites (<i>n</i> = 3)										
min	62.28	12.48	1.17	0.21	0.32	2.06	5.32	Bld	Bld	14.6	0.87
max	77.13	17.52	5.02	1.08	0.66	3.89	6.57	0.26	0.10	22.4	1.43
ave	71.43	14.52	2.50	0.52	0.48	2.87	5.79	0.09	0.03	17.7	1.09
	Altered granites and tectonites (<i>n</i> = 27)										
min	69.97	1.84	0.82	0.04	0.03	0.03	0.41	Bld	Bld	4.1	0.31
max	94.47	16.86	3.09	0.66	8.32	4.02	6.86	1.32	5.10	1154.0	3.47
ave	80.12	10.06	1.50	0.27	0.90	0.99	4.08	0.45	0.32	402.4	1.53

Notes: “Bld” in the table, body text, and appendix indicates that the element content is below the detection limit, and “*n*” is the number of samples with effective analysis results. The high U content (>1000 ppm) is assumed to be 1000 ppm for the calculation of the average U content.

4.2. Trace Element Contents

The analytical results for some trace elements from this study, as well as some previous data, are summarized in Table 3 and Appendix B Table A2. The average contents of most trace elements in altered granite are similar to those of fresh granite, except for significantly high average contents of U (4.1–1154.0 ppm, average 402.4 ppm), Pb (3.6–307.0 ppm, average 117.2 ppm), Mo (0.07–194.00 ppm, average 15.76 ppm), and Sb (0.09–9.85 ppm, average 1.14 ppm) (Figure 3i–k). Figure 4 shows primitive-mantle and chondrite normalized [31] trace-element and rare-earth-element (REE) patterns for the granite samples and other fresh granite data from previous researchers [9,15]. The primitive-mantle-normalized trace-element spider patterns show depletions in Ba, Th, Nb, Sr, and Tb and enrichment in Cs, W, U, Pb, Mo, Sb, and Li for the altered granites versus the fresh granites (Figure 4a).

4.3. Rare Earth Element Contents

The analysis results for the rare earth elements (REEs) from this study, as well as previous data, are summarized in Table 4 and Appendix C Table A3. The fresh granites have total REE (Σ REE) contents of 140.86–449.35 ppm (average 218.83 ppm), light REE (LREE) contents of 111.35–401.08 ppm (average 190.17 ppm) contents, and heavy REE (HREE) contents of 13.13–48.27 ppm (average 28.66 ppm) contents. However, the altered granites and tectonites have lower Σ REE and LREE contents, and higher HREE contents (22.96–250.99 ppm (average 145.48 ppm), 19.59–194.47 ppm (average 108.26 ppm), and 3.37–87.96 ppm (average 37.22 ppm), respectively). The fresh granites have higher LREE/HREE ratio values (3.42–12.05, average 7.08) than do the altered granites and tectonites (0.76–11.12, average 3.75). The chondrite-normalized REE patterns of the granite samples show a strongly negative Eu anomaly and depletion in HREE. Compared with the fresh granites, the HREE content of MS and OBS increases significantly (Figure 4b).

Table 3. Geochemical summary of selected trace elements and REEs (ppm) of SJOF granite samples.

	Cs	Tl	Rb	Ba	W	Th	Nb	Ta	Pb
Fresh granites (<i>n</i> = 3)									
Min	13.85	2.5	505	108.5	187	25.7	17.5	3.3	41.0
Max	27.40	2.9	514	203.0	830	117.0	31.9	5.4	48.4
Average	20.52	2.7	509	171.2	569	57.6	25.7	4.4	43.7
Altered granites and tectonites (<i>n</i> = 27)									
Min	3.26	0.49	55	17.7	108	4.7	2.1	1.4	3.6
Max	101.50	5.18	933	238.0	1620	62.2	38.1	51.0	307.0
Average	34.63	2.81	488	97.4	608	31.5	19.4	6.6	117.2
	Mo	Sr	Zr	Hf	Sn	Sb	Tb	Li	Y
Fresh granites (<i>n</i> = 3)									
Min	0.28	31.2	99.0	3.4	13.1	0.06	0.66	59.8	18.1
Max	0.45	47.8	330.0	10.7	29.0	0.11	2.46	154.0	68.6
Average	0.38	40.7	177.3	6.1	21.1	0.09	1.53	114.3	46.4
Altered granites and tectonites (<i>n</i> = 27)									
Min	0.07	6.5	8.0	0.3	2.4	0.09	0.17	12.1	6.0
Max	194.00	149.5	143.0	6.3	37.9	9.85	3.57	510.0	179.5
Average	15.76	34.1	76.3	3.3	14.1	1.14	1.63	147.2	65.8

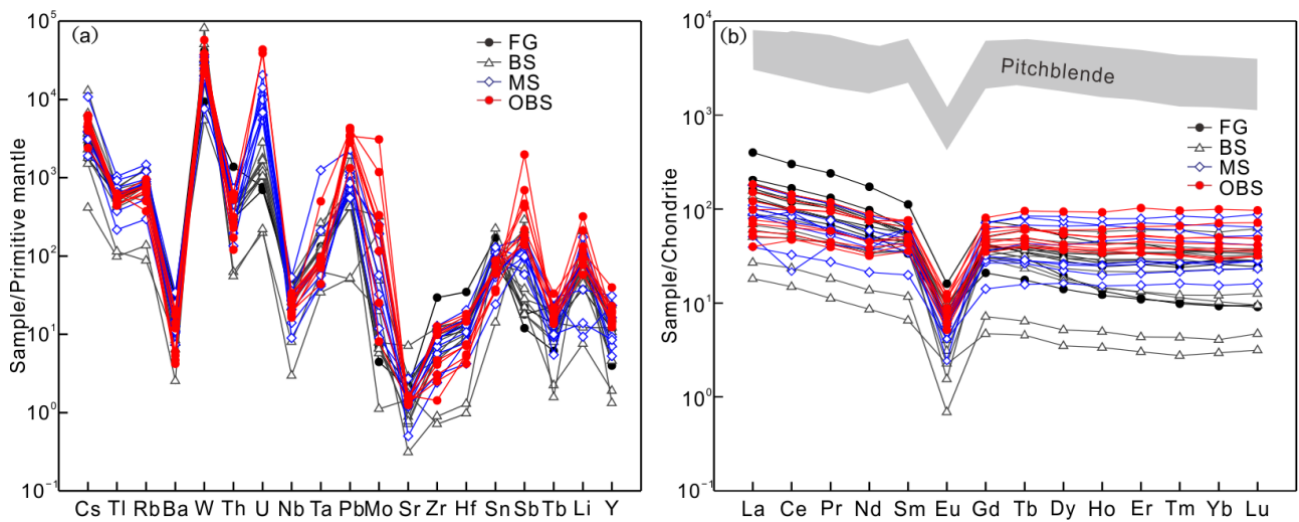


Figure 4. (a) Primitive-mantle-normalized trace element spider diagram and (b) chondrite-normalized REE diagram for the SJOF granite samples with different U contents. Note: The normalization values are from Sun and McDonough [31], and the pitchblende data are from Chen et al. [4].

the Ca content of the altered granites is variable and is highly enriched in some individual mineralized samples. The Ca released by the metasomatism of feldspar-group minerals (see reaction 1) may precipitate in the form of calcite (from a CO₂-rich fluid) and/or fluorite [28]. S mainly occurs in pyrite, chalcopyrite, and other base metal sulfides and is an important reductant for the granite-related U mineralization (see reaction 2, Figure 5d,f,g) [4,34]. Pyrite and pitchblende are usually deposited alternately in mineralization [35], resulting in the gradual increase of pyrite content in the altered granite. Microscopic observations also show that the pyrite contents in the BS and MS are significantly less than those in the OBS. However, EPMA and LA-ICP-MS analyses show that, compared to the euhedral-subhedral pyrites in BS and MS, the subhedral-anhedral pyrites in OBS are depleted in S (Figure 5e) [4]. The relative depletion in S of pyrite from mineralized material may promote the continuous formation and precipitation of base metal sulfides in these mineralized regions. The F content of granite samples is variable due to the variable development of fluorite in granite. F mainly occurs in a fluoride complex in the mineralizing fluid. Destabilization of the fluoride complex in the mineralizing fluid resulted in precipitation of uraninite and formation of fluorite from the F and Ca, with the fluorite being surrounded by the uranium minerals (Figure 5i). The color of fluorite associated with pitchblende was initially light purplish or turquoise; however, it would gradually turn darker to dark-purple after intense irradiation by the uranium minerals (Figure 2c,g) [36,37]. Therefore, dark-purple fluorite is an important prospecting indicator for U mineralization. Aluminum in fresh granite mainly occurs in the rock-forming minerals prone to clay mineral-group alteration, such as biotite, plagioclase, and K-feldspar (see reaction (1), (3)). Alumina is a very conservative component in granite; thus, the clay mineral-group alteration (e.g., chloritization, kaolinitization) of Al-bearing minerals usually does not lead to gains or losses of Al in the alteration from fresh granite to altered granite. However, clay minerals (especially those present in mineralization-controlling faults) can be easily destabilized by post-mineralization fluids, resulting in loss of Al from the altered granite. Compared with fresh granites, most altered granites that contain strongly developed limonite and hematite also show strong depletion in Fe. However, individual OBS show high enrichment in Fe (Figures 3c and 5c). The hematite, which is closely associated with uranium mineralization, has a high Fe²⁺/Fe³⁺ ratio. Fe²⁺ may be released from pyrite and other ferrous Fe-bearing minerals, while precipitation of ferric (Fe³⁺) Fe-bearing minerals results from the oxidation of Fe²⁺. The Mg in the altered granite is also as strongly depleted as Fe and shows slight enrichment with increasing U content. This enrichment may be due to the release of Mg²⁺ from biotite and the adsorption of U by chlorite during the chloritization alteration (Figure 5a,b, and reaction 3) [38]. K and Na show strong and continuous relative loss from altered rocks, which is related to the transformation of rock-forming minerals (biotite and feldspar) into clay minerals (chlorite, illite, and montmorillonite; see reaction 3). For example, the EPMA results show that the K₂O content of chlorite (usually <1%) is much lower than that of biotite (usually ranging from 9% to 10%) [39]. It suggests that the H⁺-rich fluid activity in the SJOF is strong, while the alkali element activities are lower and metasomatic alteration is not well-developed. The main reason for the high Pb content in OBS is due to the decay of radioactive elements, especially U, while high contents of Mo and Sb in OBS may be brought in by the medium-high temperature mineralizing fluid derived from deep-derived thermal circulating fluids.

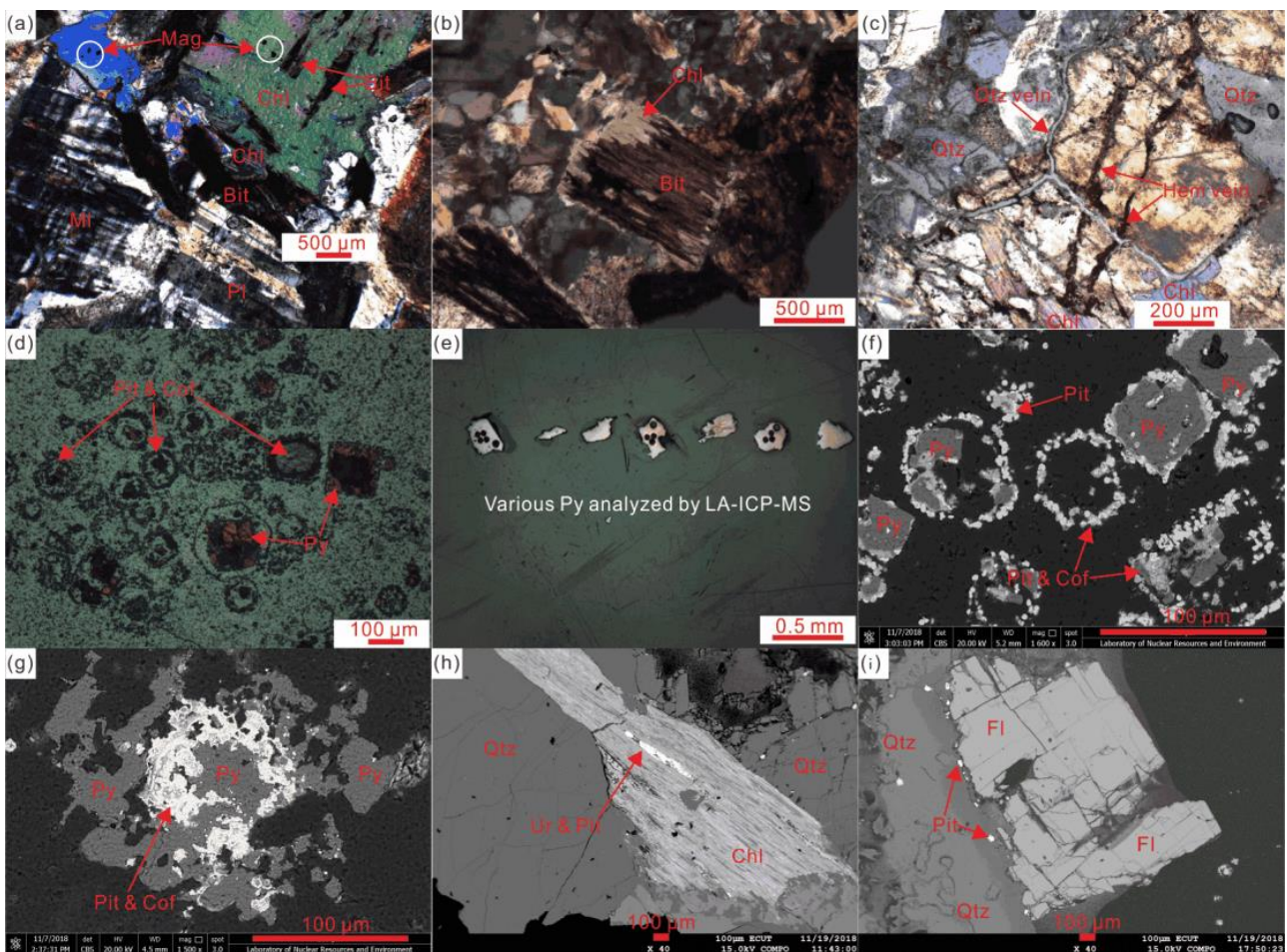


Figure 5. Representative minerals in altered SJOF granites. Notes: Images (a–e) are optical micrographs; images (f–i) are backscatter micrographs. Abbreviations: Bit—biotite; Chl—chlorite; Cof—coffinite; Fl—fluorite; Hem—hematite; Mag—magnetite; Mi—microcline; Pit—pitchblende; Pl—plagioclase; Py—pyrite; Qtz—quartz; Ur—uraninite.

5.2. Relative Migration of Trace Elements in Uranium Mineralization

Many trace elements were analyzed in this study, but only a few trace elements, including the REEs, are closely related to uranium mineralization. The average content of some trace elements (e.g., W, Mo, Sb, and Li) increases significantly with increasing U content, indicating that the mineralizing fluid moved these elements into the deposit during the mineralization process. The abundances of these elements in the SJOF granites are relatively high. For example, the fresh granite with no obvious host-rock alteration contains markedly higher W and Li contents (average 569 ppm and 114 ppm, respectively) than those of the general acidic granite (generally <10 ppm and <60 ppm, respectively). In addition, the presence of molybdenite (MoS_2) of hydrothermal genesis, stibnite (Sb_2S_3), and quartz vein-type tungsten–molybdenum (W–Mo) deposits in and around the SJOF also indicates that these trace-element abundances are relatively high [32]. These high-abundance trace elements can be regarded as prospecting indicators for U mineralization in the SJOF.

Figure 4b shows that, as the U content increases, the chondrite-normalized REE patterns of the altered granite gradually change from right-dipping profile to the gull-winged type similar to that for pitchblende. The average total REE content of altered granites gradually increases (BS, 131.0 ppm; MS, 143.9 ppm; OBS, 162.9 ppm) with degree of alteration and proximity to pitchblende. These REE patterns suggest that the REE in altered granites are gradually enriched and fractionated with the enrichment of U. The

REE and U in mineralizing fluids mainly travel together and are transported in the form of $(U, REE)O_2(CO_3)$ and $(U, REE)O_2(CO_3)$ complexes, due to their similar ionic radius [40,41]. As a consequence, REE and U are usually enriched and precipitated together during mineralization (OBS samples). However, the ionic radius of the HREEs is smaller than that of the LREEs and results in a relatively more stable HREE complex [42,43]. Therefore, during both hydrothermal alteration and mineralization in the granite plutons, the HREEs are easier to enrich in altered granites than LREEs, particularly in OBS. This leads to a gradual decrease in the LREE/HREE ratio with the enrichment of U. The analysis results show that the average LREE/HREE ratio of OBS (2.53) and pitchblende (2.46, ranging from 1.50 to 4.49; unpublished data) is significantly smaller than that of MS (3.09) and BS (5.38), showing that the altered granite with a low LREE/HREE ratio (generally <3) corresponds to a more pronounced mineralization process.

5.3. Vertical Migration of Elements in Uranium Mineralization

The granite-related U mineralization in the SJOF mainly occurs in the redox zone, i.e., the transitional part of the oxidation and reduction zones, where the uranyl complexes in fluids are prone to decomposition. Figure 6 shows that the burial depths of OBS and MS are mainly concentrated in the 100–200 m and 100–300 m ranges, respectively, while the burial depths of BS are relatively variable. It shows that most of the ore bodies in the SJOF are mostly concentrated in the burial depth of 100–300 m, which is the most favorable region for mineral exploration. The aforementioned events demonstrate that hydrothermal alteration may only aid in the development of U ore bodies in a suitable mineralization environment (redox zone) [44]. The redox zone is usually characterized by drastic changes in physicochemical conditions, such as pH and Eh values, temperature, pressure, and oxygen escape. The redox zone typically contains large amounts of mineralizing/reducing agents (e.g., reducing ions related to pyrite) that could greatly facilitate the decomposition of U complexes, the reduction of active U, the enrichment and precipitation of inert U, and finally lead to the formation of ore bodies. For example, dark-purple fluorite (CaF_2) and pyrite (FeS_2) are generally associated with uranium mineralization, and these F- and S-bearing granite samples are mostly developed between a 100 and 300 m burial depth in the redox zone (Figure 7a,b).

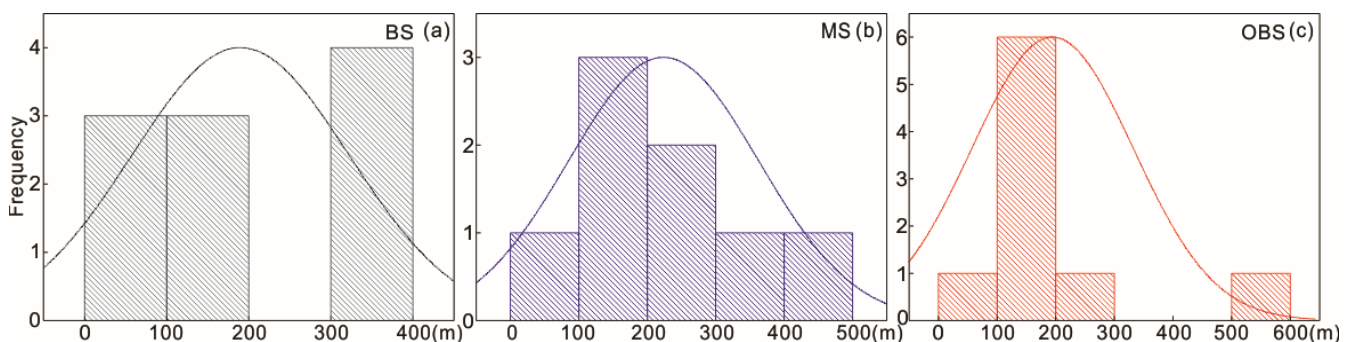


Figure 6. Histograms of burial depth versus granite sample type. (a) Barren samples, (b) Mineralized samples, (c) Ore-bearing samples.

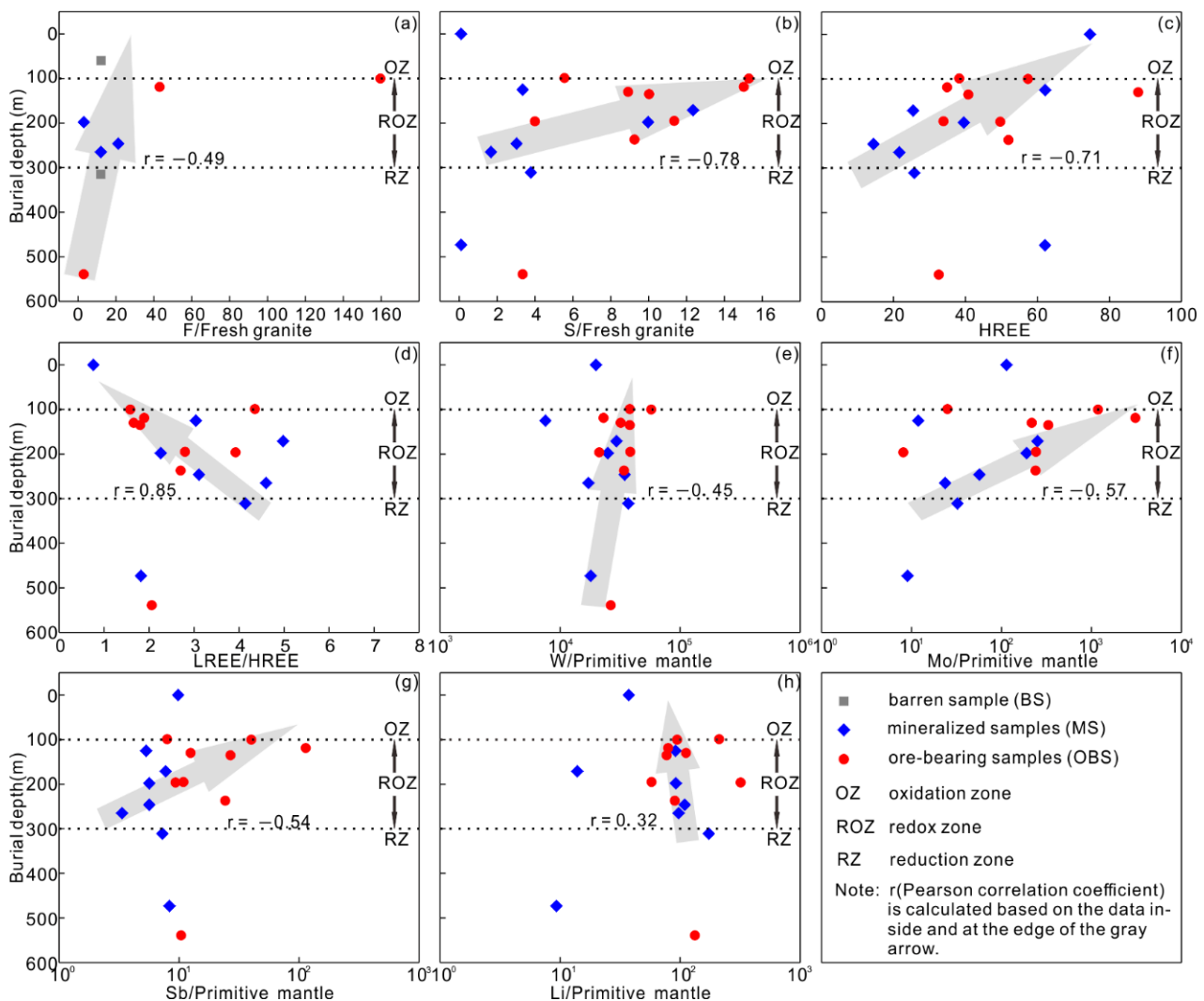


Figure 7. Scatter plots of some elements and element combinations in various altered granites versus burial depth (Bd). (a) F vs. Bd, (b) S vs. Bd, (c) HREE vs. Bd, (d) LREE/HREE vs. Bd, (e) W vs. Bd, (f) Mo vs. Bd, (g) Sb vs. Bd, (h) Li vs. Bd.

There are linear correlations between some geochemical indicators and the depth of mineralization. The S content in most MS and OBS steadily increases with decreasing burial depth, as illustrated in the 100–300 m burial depth interval (Figure 7b), demonstrating that S is an important mineralization agent in the mineralization process. The HREE in most MS and OBS also gradually increases with decreasing burial depth; however, the LREE/HREE ratio decreases (Figure 7c,d), indicating that HREE is more likely to be enriched in the oxidation zone and redox zone than LREE. Some trace elements (e.g., W, Mo, Sb, and Li), potentially useable as prospecting indicators, in MS and OBS show no obvious linear relationship with burial depth ($|r| < 0.6$, Figure 7e–h), thus indicating that their enrichment does not appear to be causally related to the U mineralization. However, with the decreasing burial depth in the redox zone, the content of these elements (e.g., W, Mo, Sb, and Li) in OBS increases more significantly than in MS, implying that these trace elements may have come from deep-derived fluid.

5.4. Metallogenic Process and Hydrothermal Alteration

The formation of U-rich granites, extensional tectonic settings, movement of fluids carrying the mineralization components, and extensive development of hydrothermal alterations of the host-rocks were the combined geological events that led to the formation

of U deposits in the SJOF. The SJOF experienced a large-scale granite intrusion event in the Late Jurassic (162–148 Ma) and a large-scale extensional tectonic event beginning in the Early Cretaceous (136 Ma) [45–47]. The long-term tectonic activities and various superimposed hydrothermal alterations promoted lithologic, mineral, and elemental changes in the granites:

- (1) The formation and subsequent transformation of alteration minerals, such as K-feldspar, chlorite, kaolinite, illite, calcite, dark-purple fluorite, pyrite, and hematite;
- (2) The release of large amounts of U through dissolution of U-bearing accessory minerals (uraninite, zircon, apatite, allanite, biotite, monazite, epidote, etc.) [48–51];
- (3) The formation of many microfractures in rocks and mineral grains that are filled with neoformed minerals under continuous fluid pressure that form fine veins, such as microcrystalline quartz veins, hematite veins, fluorite veins, and calcite veins;
- (4) The reduction of the compressive strength and the increase in the porosity of the rocks as a result of these mineralogical changes promoted the movement of U from altered granite to a structural/chemical trap (faults) and the gains and losses of major and trace elements in the altered granites;
- (5) The contents of some elements are positively correlated with that of U. These elements either act as important reducing agents (reduction of uranyl U) or have similar geochemical properties (formation of various complexes) and geochemical behavior (co-enrichment and/or co-precipitation in the redox zone) to U.

The critical prerequisites for the formation of granite-related U deposit may be briefly summarized as the source, migration, and enrichment of U, corresponding to U-rich granite, thermal sources promoting the flow of mineralizing fluid, and suitable mineralization zone, respectively. We have found the the following to be true: (1) The Sanjiangkou granite with high U content (14.6–22.4 ppm) was the main U source of SJOF. (2) The large-scale hydrothermal alterations promoted the release and migration of active U, and the superimposed hydrothermal alterations facilitated the enrichment of U. (3) The multisource mineralizing fluid, which was rich in oxygen and uranyl U, continuously extracted and/or transferred high-abundance trace elements in granite while flowing upward along mineralization-controlling faults [50,51]. (4) U complexes in the mineralizing fluid were destabilized and decomposed continuously under a medium–low temperature (110–260 °C), reducing environment [4,50–53]; however, the high content of trace elements, such as W, Mo, and Sb, implies that the mineralizing fluid may be partially derived from medium–high temperature fluids (partial heat source). (5) U and other trace elements (Mo, Sb, REE, etc.) were simultaneously enriched and precipitated in the redox zone (also a structural/chemical trap), which is mainly concentrated in the 100–300 m burial depth, and U precipitated in several uranium minerals (e.g., pitchblende, coffinite, and thorite).

6. Conclusions

- (1) The U-rich Jurassic granite plutons can be regarded as the primary U sources for the SJOF U mineralizations, one of the prerequisites for the formation of uranium deposits. The relative movement of elements or element combinations in the altered granite, such as S, Na + K, Al, Mg, Mo, Sb, and LREE/HREE, is positively or negatively correlated with U mineralization. The migration of these elements corresponds to some important hydrothermal alterations associated with U mineralization (e.g., silicification, pyritization, dark-purple fluoritization, carbonation, and hematitization and some neoformed minerals (e.g., microcrystalline quartz, K-feldspar, chlorite, calcite, hematite, molybdenite, stibnite, kaolinite, illite, and pyrophyllite). Various hydrothermal alterations promoted the migration and enrichment of U, major and trace elements, another important prerequisite for the formation of uranium deposits.
- (2) The ore-bearing altered granites (OBS, ore) are characterized by a low LREE/HREE ratio (<3); enrichment of W, Mo, Sb, and Li; and development of base metal sulfide minerals, such as pyrite, molybdenite, and stibnite. The precipitation and enrichment

mechanisms of U and the REE, especially the HREE, are similar in mineralized altered granites (MS) and ore-bearing altered granites (OBS).

- (3) The main mineralized redox zone of the SJOF is concentrated in the burial depth range of 100–300 m and is superimposed on a variety of hydrothermal alterations that are favorable for mineralization. The relatively high W, Mo, Sb, Li, and HREE contents in the upper part of the redox zone appear to better indicate the presence of U mineralization. Some trace elements (W, Mo, Sb, etc.) present in the ore suggest that the mineralizing fluids may be mixed with medium–high temperature fluids (a potential heat source), but further work is needed.

Author Contributions: X.C., D.M. and C.W. conceived of this contribution; X.C. and B.J. wrote the paper with contributions from J.Q. and B.L.; X.C. and B.L. performed the experiments and analyzed the data. All authors have read and agreed to the published version of the manuscript.

Funding: This work was funded by the Science and Technology Research Project of China Nuclear Geology (No. 2110400024), Cooperative Uranium Geological Exploration Foundation of China National Nuclear Corporation (No. J2012-03), Youth Scientific Research Project of Geological Bureau of Hunan Province (No. 2021YSP-07), Key R & D project of Hunan Provincial Science and Technology Department (No. 2019SK2261); Scientific research project of Geological Bureau of Hunan Province (No. HNGSTP202105), and project supported by the open fund of the Key Laboratory of Metallogenic Prediction of Nonferrous Metals and Geological Environment Monitoring, Ministry of Education (No. 2021YSJS04).

Data Availability Statement: Data is contained within the article.

Acknowledgments: We are grateful for the analysis results provided by the ALS Laboratory Group, Mineral Division–ALS Chemex, and the suggestions, changes, and comments provided by the reviewers and the academic editor.

Conflicts of Interest: The authors declare no conflict of interest.

Appendix A

Table A1. Major element oxide (wt%) and U (ppm) analyses of SJOF granite samples.

Sample No.	SiO ₂	Al ₂ O ₃	Fe ₂ O _{3T}	MgO	CaO	Na ₂ O	K ₂ O	SO ₃	F	U	LOI	Total
DI	0.01	0.01	0.01	0.01	0.01	0.01	0.01	0.01	0.1	0.05	0.01	
ZS07	94.47	1.84	1.32	0.04	0.29	0.34	0.64	0.03	Bld	4.1	0.31	99.34
ZS09	83.47	9.78	1.05	0.17	0.31	0.05	3.39	0.08	Bld	34.7	1.41	99.74
SBW13	74.87	13.57	1.17	0.21	0.45	2.66	5.32	Bld	0.1	14.6	0.96	99.33
SBW24	76.35	12.24	0.91	0.12	1.18	3.03	4.64	0.14	Bld	37.2	1.34	99.97
SBW26	71.59	14.97	2.04	0.26	1.16	3.04	5.45	0.02	Bld	35.0	0.84	99.41
SBW28	71.58	14.53	1.83	0.61	1.91	0.1	5.71	Bld	Bld	21.5	3.47	99.78
JLJ02	69.97	16.86	2.50	0.66	0.25	0.67	6.65	0.30	Bld	242.0	2.12	100.00
JLJ03	78.49	11.68	1.27	0.29	0.41	1.28	4.78	0.89	0.1	115.0	1.33	100.53
JLJ04	75.46	12.42	2.33	0.21	0.90	2.17	5.45	0.15	0.4	132.0	0.79	100.32
JLJ07	78.01	4.39	1.09	0.36	8.32	0.03	1.86	1.32	5.1	>1000	3.38	103.88
JLJ08	74.99	13.1	2.01	0.45	0.36	0.16	6.00	0.36	Bld	813.0	2.10	99.56
JLJ09	77.13	12.48	1.3	0.28	0.32	2.06	5.47	0.01	Bld	22.4	0.87	99.95
JLJ10	79.57	10.58	1.39	0.37	0.41	0.23	4.87	0.50	Bld	1007.0	1.74	99.69
JLJ11	77.59	10.78	3.09	0.38	0.26	0.78	5.10	0.80	Bld	1154.0	1.07	99.89
JLJ13	88.09	5.74	1.37	0.22	0.18	0.06	2.25	0.90	Bld	>1000	1.13	99.97
JLJ17	83.71	5.85	1.74	0.28	2.62	0.09	2.69	1.32	1.4	>1000	2.33	102.05
JLJ24	85.95	7.75	1.04	0.24	0.22	0.08	2.93	0.34	Bld	145.0	1.41	99.97
JLJ26	62.28	17.52	5.02	1.08	0.66	3.89	6.57	0.26	Bld	16.0	1.43	98.94

Table A1. Cont.

Sample No.	SiO ₂	Al ₂ O ₃	Fe ₂ O _{3T}	MgO	CaO	Na ₂ O	K ₂ O	SO ₃	F	U	LOI	Total
DI	0.01	0.01	0.01	0.01	0.01	0.01	0.01	0.01	0.1	0.05	0.01	
JLJ27	82.06	8.69	1.96	0.29	0.19	0.12	4.49	0.83	Bld	>1000	1.23	99.91
JLJ28	84.16	8.30	1.21	0.31	0.19	0.10	3.91	1.01	Bld	>1000	1.48	100.70
JLJ29	78.96	10.78	1.23	0.16	0.61	2.48	4.28	0.09	Bld	28.2	0.97	99.60
JLJ30	90.58	3.75	1.14	0.11	1.20	0.04	1.52	0.27	0.7	430.0	1.21	100.53
JLJ31	76.71	12.05	1.19	0.37	0.53	0.97	5.49	1.10	Bld	207.0	2.12	100.55
JLJ33	81.26	9.94	1.49	0.34	0.5	0.22	4.05	0.30	0.1	909.0	1.83	100.06
XCD02	71.75	15.84	1.33	0.28	0.55	4.02	4.89	0.44	Bld	25.1	1.40	100.52
XCD07	82.51	10.05	0.88	0.27	0.22	0.12	4.27	Bld	Bld	21.9	1.52	99.85
XCD09	71.64	15.70	0.82	0.08	0.19	3.24	6.86	0.01	Bld	296.0	0.99	99.54
XCD12	93.84	1.87	2.13	0.09	0.73	0.08	0.41	0.85	0.4	4.6	0.70	101.11
XCD13	76.23	12.88	1.14	0.17	0.66	3.16	4.52	Bld	0.4	59.0	0.96	100.20
XCD15	84.12	9.39	0.93	0.18	0.03	0.07	3.04	0.01	Bld	143.0	2.23	100.05

Note: DI is the detection limit of element.

Appendix B

Table A2. Selected trace element contents (ppm) of SJOF granite samples.

Sample No.	Cs	Tl	Rb	Ba	W	Th	Nb	Ta	Pb
DI	0.01	0.02	0.20	0.50	0.10	0.05	0.10	0.10	0.50
ZS07	3.26	0.49	86.8	17.7	1620	5.3	5.7	2.6	3.6
ZS09	33.2	2.25	498	44.6	496	29.3	15.7	4.4	29.2
SBW13	27.4	2.63	514	203.0	830	25.7	27.6	5.4	41.0
SBW24	29.3	3.58	566	122.5	660	36.0	37.5	8.5	44.2
SBW26	28.7	2.70	522	229.0	436	35.4	27	5.0	44.4
SBW28	101.50	3.64	844	130.5	108	36.7	28.3	5.3	40.2
JLJ02	85.2	5.18	933	124.5	151	52.7	21.9	3.6	84.7
JLJ03	30.0	3.23	526	106.0	499	22.9	10.0	1.7	70.5
JLJ04	24.3	2.92	566	88.7	344	50.5	19.1	3.1	76.1
JLJ07	18.9	3.14	238	41.8	1150	14.5	13.6	2.9	307.0
JLJ08	46.8	3.04	607	123.0	424	53.0	23.9	3.8	304.0
JLJ09	20.3	2.50	508	108.5	690	30.1	17.5	3.3	48.4
JLJ10	31.6	2.58	480	144.0	760	44.4	20.7	3.0	94.4
JLJ11	35.7	2.88	500	124.5	640	49.2	22.9	3.7	211.0
JLJ13	49.0	2.31	402	32.8	760	10.2	11.7	20.5	284.0
JLJ17	35.0	3.07	319	29.4	460	19.6	14.1	1.8	243.0
JLJ24	35.3	1.87	336	73.1	740	30.0	14.9	2.3	51.7
JLJ26	13.85	2.90	505	202.0	187	117.0	31.9	4.6	41.8
JLJ27	38.6	3.11	490	83.6	680	49.1	19.2	4.0	246.0
JLJ28	44.5	2.20	441	96.7	767	22.5	12.5	3.6	201.0
JLJ29	14.1	2.09	404	125.5	660	44.7	18.3	3.3	45.8
JLJ30	24.7	1.08	187	51.4	690	16.6	6.4	1.8	63.6
JLJ31	30.5	3.75	604	172.0	590	62.2	19.4	3.8	60.1
JLJ33	49.3	2.72	524	37.4	528	26.8	17.4	3.7	241.0
XCD02	18.1	2.90	534	53.8	318	27.0	29.1	8.0	135.5
XCD07	23.8	2.75	498	102.5	586	24.6	24.8	4.8	29.5
XCD09	15.0	4.62	758	238.0	360	44.5	25.6	8.6	39.1
XCD12	11.85	0.57	55.2	59.0	1010	4.7	2.1	1.4	3.7
XCD13	52.4	3.78	801	102.0	591	26.1	24.1	10.8	48.2
XCD15	24.3	3.29	468	76.7	397	11.4	38.1	51.0	161.5

Table A2. Cont.

Sample No.	Mo	Sr	Zr	Hf	Sn	Sb	Tb	Li	Y
D1	0.05	0.10	2.00	0.20	0.20	0.05	0.01	0.20	0.10
ZS07	1.24	6.5	10	0.4	19.5	0.11	0.24	12.1	8.6
ZS09	0.42	18.6	72	3.1	12.9	0.32	1.19	103.0	48.4
SBW13	0.45	47.8	103	3.4	21.1	0.06	0.66	154.0	18.1
SBW24	0.36	42.3	109	4.2	22.0	0.14	1.07	93.0	33.5
SBW26	0.5	149.5	136	4.4	21.0	0.09	0.97	71.3	20.8
SBW28	0.07	30.9	141	4.6	18.0	0.09	0.86	125.0	20.8
JLJ02	0.75	27.0	143	6.3	21.8	0.46	2.53	146.5	107.0
JLJ03	12.00	30.4	63	2.4	9.1	0.49	1.60	147.5	74.5
JLJ04	1.49	30.3	99	4.0	19.0	0.29	0.99	155.5	32.0
JLJ07	74.30	29.3	34	1.6	6.3	3.47	2.21	151.0	104.5
JLJ08	0.51	28.4	142	5.6	10.1	0.81	2.30	510.0	75.3
JLJ09	0.42	31.2	99	4.2	13.1	0.11	1.46	59.8	52.5
JLJ10	1.58	29.9	116	4.6	12.6	0.69	1.71	338.0	56.3
JLJ11	13.65	30.4	122	5.3	12.4	1.08	3.57	179.0	179.5
JLJ13	20.90	34.6	16	1.7	14.5	2.32	1.87	123.5	84.7
JLJ17	194.00	26.3	46	2.3	5.9	9.85	1.48	127.0	60.9
JLJ24	2.04	25.2	78	3.3	10.2	0.63	1.05	277.0	42.0
JLJ26	0.28	43.1	330	10.7	29.0	0.09	2.46	129.0	68.6
JLJ27	15.05	31.5	110	4.5	12.5	2.10	2.37	144.5	90.7
JLJ28	15.25	33.5	52	2.2	6.3	0.94	1.60	92.5	67.9
JLJ29	0.41	32.8	90	3.7	13.3	0.19	1.81	112.0	71.2
JLJ30	3.58	25.3	34	1.3	4.1	0.49	0.59	174.5	23.9
JLJ31	15.85	34.3	120	4.8	10.1	0.67	1.07	22.2	38.5
JLJ33	7.29	28.3	28	1.3	15.0	0.9	1.48	212.0	64.3
XCD02	3.05	60.3	52	2.9	14.9	0.34	1.52	19.4	55.4
XCD07	19.90	14.9	58	2.6	15.7	1.07	1.35	132.5	55.8
XCD09	0.57	57.0	94	4.7	9.9	0.72	3.05	14.9	106.0
XCD12	13.20	36.8	8	0.3	2.4	1.44	0.17	330.0	6.0
XCD13	0.49	16.2	61	4.2	37.9	0.14	2.23	100.5	107.0
XCD15	7.15	10.5	27	2.5	22.0	0.85	3.15	59.7	141.5

Appendix C

Table A3. REE contents (ppm) and parameters of SJOF granite samples.

Sample No.	La	Ce	Pr	Nd	Sm	Eu	Gd	Tb	Dy	Ho	Er
D1	0.10	0.10	0.03	0.10	0.03	0.03	0.05	0.01	0.05	0.01	0.03
ZS07	6.4	14.4	1.73	6.4	1.79	0.04	1.48	0.24	1.31	0.28	0.72
ZS09	16.0	36.2	4.36	16.4	5.50	0.23	6.10	1.19	7.61	1.65	4.84
SBW13	30.0	59.0	7.45	25.8	5.04	0.44	4.30	0.66	3.57	0.68	1.81
SBW24	32.0	61.4	7.62	28.0	6.76	0.42	6.20	1.07	5.92	1.23	3.54
SBW26	44.4	87.0	11.10	38.4	7.83	0.58	6.40	0.97	4.65	0.83	2.14
SBW28	44.6	88.2	10.65	36.5	7.61	0.53	6.00	0.86	4.36	0.81	2.19
JLJ02	42.4	85.0	10.80	39.7	10.60	0.35	12.60	2.53	16.70	3.80	11.80
JLJ03	20.7	40.1	4.97	18.1	5.17	0.33	7.30	1.60	10.45	2.58	8.02
JLJ04	20.9	44.1	5.95	22.0	6.19	0.36	5.50	0.99	5.61	1.12	3.43
JLJ07	16.5	39.0	5.49	21.1	7.89	0.65	10.25	2.21	15.15	3.42	10.75
JLJ08	43.4	87.3	11.15	40.9	11.20	0.52	11.50	2.30	13.55	2.82	8.52
JLJ09	24.2	50.0	6.47	23.6	6.75	0.33	7.40	1.46	8.59	1.85	5.65
JLJ10	36.0	75.6	9.62	35.0	9.78	0.36	9.70	1.71	10.25	2.12	6.53
JLJ11	28.7	61.3	8.92	34.7	11.85	0.63	16.60	3.57	23.80	5.22	17.00
JLJ13	13.7	33.1	4.00	15.8	6.39	0.41	8.90	1.87	10.85	2.36	7.40
JLJ17	12.3	29.5	3.68	14.6	5.41	0.30	7.10	1.48	9.51	2.04	6.35

Table A3. Cont.

Sample No.	La	Ce	Pr	Nd	Sm	Eu	Gd	Tb	Dy	Ho	Er
JLJ24	23.8	50.8	5.71	20.9	5.44	0.24	5.80	1.05	6.80	1.46	4.61
DI	0.10	0.10	0.03	0.10	0.03	0.03	0.05	0.01	0.05	0.01	0.03
JLJ26	94.6	185.0	22.80	80.6	17.15	0.93	15.35	2.46	13.05	2.45	7.06
JLJ27	23.3	60.9	8.80	35.0	11.40	0.72	13.30	2.37	13.70	2.84	8.77
JLJ28	18.1	42.4	5.60	20.9	7.32	0.47	8.30	1.60	9.57	2.05	5.62
JLJ29	36.5	79.6	9.51	35.1	9.73	0.39	9.73	1.81	11.30	2.44	7.01
JLJ30	9.3	19.9	2.61	9.9	3.04	0.24	2.90	0.59	4.11	0.86	2.56
JLJ31	26.0	58.1	7.18	27.6	7.41	0.39	6.50	1.07	6.45	1.41	4.27
JLJ33	9.4	28.4	4.30	18.0	6.70	0.34	8.00	1.48	9.13	1.89	5.60
XCD02	21.1	47.0	5.81	22.4	6.97	0.18	7.63	1.52	9.74	1.94	5.75
XCD07	14.1	32.2	4.12	15.6	5.49	0.13	6.60	1.35	9.02	1.89	5.67
XCD09	18.8	57.0	5.33	21.9	9.48	0.39	14.65	3.05	18.80	3.80	10.30
XCD12	4.3	9.1	1.06	4.0	1.00	0.13	0.97	0.17	0.89	0.19	0.50
XCD13	11.8	30.1	4.09	16.6	7.32	0.09	10.50	2.23	15.00	3.26	9.87
XCD15	12.0	13.2	3.96	17.6	9.57	0.14	14.70	3.15	21.10	4.46	13.10
LHF [9]	39.0	77.2	10.13	36.64	8.69	0.46	8.56	1.31	7.64	1.51	4.53
KY6 [15]	49.1	101.9	12.50	45.46	9.56	0.54	7.41	1.14	4.94	0.76	1.86
12DL [15]	29.6	61.6	7.60	30.38	8.32	0.35	8.17	1.40	8.20	1.59	4.70
15DL [15]	36.4	72.0	9.71	34.90	8.60	0.37	8.72	1.29	7.10	1.38	4.25
Sample No.	Tm	Yb	Lu	∑REE	LREE	HREE	L/H	Sm/Nd	Y/Ho	δEu	δCe
DI	0.01	0.03	0.01								
ZS07	0.11	0.69	0.12	35.71	30.76	4.95	6.21	0.28	30.71	0.08	1.06
ZS09	0.74	4.45	0.73	106.00	78.69	27.31	2.88	0.34	29.33	0.12	1.06
SBW13	0.26	1.62	0.23	140.86	127.73	13.13	9.73	0.20	26.62	0.29	0.97
SBW24	0.56	3.89	0.59	159.20	136.20	23.00	5.92	0.24	27.24	0.20	0.96
SBW26	0.29	1.76	0.24	206.59	189.31	17.28	10.96	0.20	25.06	0.25	0.96
SBW28	0.31	2.06	0.32	205.00	188.09	16.91	11.12	0.21	25.68	0.24	0.99
JLJ02	1.74	11.35	1.62	250.99	188.85	62.14	3.04	0.27	28.16	0.09	0.97
JLJ03	1.16	7.37	1.05	128.90	89.37	39.53	2.26	0.29	28.88	0.16	0.97
JLJ04	0.55	3.85	0.59	121.14	99.50	21.64	4.60	0.28	28.57	0.19	0.97
JLJ07	1.69	12.05	1.82	147.97	90.63	57.34	1.58	0.37	30.56	0.22	1.00
JLJ08	1.25	8.49	1.23	244.13	194.47	49.66	3.92	0.27	26.70	0.14	0.97
JLJ09	0.89	5.87	0.85	143.91	111.35	32.56	3.42	0.29	28.38	0.14	0.98
JLJ10	0.95	6.12	0.89	204.63	166.36	38.27	4.35	0.28	26.56	0.11	1.00
JLJ11	2.46	16.85	2.46	234.06	146.10	87.96	1.66	0.34	34.39	0.14	0.94
JLJ13	1.10	7.25	1.05	114.18	73.40	40.78	1.80	0.40	35.89	0.17	1.10
JLJ17	0.94	6.53	0.93	100.67	65.79	34.88	1.89	0.37	29.85	0.15	1.08
JLJ24	0.69	4.68	0.70	132.68	106.89	25.79	4.14	0.26	28.77	0.13	1.07
JLJ26	0.92	6.05	0.93	449.35	401.08	48.27	8.31	0.21	28.00	0.18	0.98
JLJ27	1.24	8.49	1.24	192.07	140.12	51.95	2.70	0.33	31.94	0.18	1.04
JLJ28	0.83	5.11	0.80	128.67	94.79	33.88	2.80	0.35	33.12	0.18	1.03
JLJ29	1.01	6.38	0.96	211.47	170.83	40.64	4.20	0.28	29.18	0.12	1.05
JLJ30	0.41	2.62	0.41	59.45	44.99	14.46	3.11	0.31	27.79	0.25	0.99
JLJ31	0.68	4.35	0.72	152.13	126.68	25.45	4.98	0.27	27.30	0.17	1.04
JLJ33	0.81	4.88	0.80	99.73	67.14	32.59	2.06	0.37	34.02	0.14	1.10
XCD02	0.88	5.34	0.83	137.09	103.46	33.63	3.08	0.31	28.56	0.08	1.04
XCD07	0.85	5.05	0.80	102.87	71.64	31.23	2.29	0.35	29.52	0.07	1.04
XCD09	1.52	8.64	1.33	174.99	112.90	62.09	1.82	0.43	27.89	0.10	1.40
XCD12	0.07	0.50	0.08	22.96	19.59	3.37	5.81	0.25	31.58	0.40	1.05
XCD13	1.52	9.65	1.57	123.60	70.00	53.60	1.31	0.44	32.82	0.03	1.06
XCD15	2.14	13.70	2.23	131.05	56.47	74.58	0.76	0.54	31.73	0.04	0.47
LHF [9]	0.69	4.77	0.71	201.86	172.14	29.72	5.79	0.24	27.93	0.16	0.95
KY6 [15]	0.25	1.58	0.24	237.26	219.08	18.18	12.05	0.21	28.11	0.20	1.01
12DL [15]	0.64	4.99	0.72	168.26	137.85	30.41	4.53	0.27	28.60	0.13	1.01
15DL [15]	0.61	4.38	0.62	190.30	161.95	28.35	5.71	0.25	26.86	0.13	0.94

Notes: L/H = LREE/HREE; δEu = Eu_N/(Sm_N·Gd_N)^{1/2}; δCe = Ce_N/(La_N·Pr_N)^{1/2}.

References

1. Liu, G.Q.; Zhao, K.D.; Jiang, S.Y.; Chen, W. In-situ sulfur isotope and trace element analysis of pyrite from the Xiawang uranium ore deposit in South China: Implication for ore genesis. *J. Geochem. Expl.* **2018**, *195*, 49–65. [[CrossRef](#)]
2. Mao, J.W.; Xiong, B.K.; Liu, J.; Pirajno, F.; Cheng, Y.B.; Ye, H.S.; Song, S.W.; Dai, P. Molybdenite Re/Os dating, zircon U–Pb age and geochemistry of granitoids in the Yangchuling porphyry W–Mo deposit (Jiangnan tungsten ore belt), China: Implications for petrogenesis, mineralization and geodynamic setting. *Lithos* **2017**, *286–287*, 35–52. [[CrossRef](#)]
3. Deng, P.; Ren, J.S.; Ling, H.F.; Shen, W.Z.; Sun, L.Q.; Zhu, B.; Tan, Z.Z. SHRIMP zircon U–Pb ages and tectonic implications for Indosinian granitoids of southern Zhuguangshan granitic composite, South China. *Chin. Sci. Bull.* **2012**, *57*, 1231–1241, (In Chinese with English Abstract). [[CrossRef](#)]
4. Chen, X.; Liu, X.D.; Qin, J.N.; Jiang, B.J. Constraints on granite-related uranium mineralization in the Sanjiu uranium ore field, SE China provided by pyrite mineralogy, major and trace elements, S–He–Ar isotopes. *Acta Geochim.* **2020**, *39*, 471–486. [[CrossRef](#)]
5. Xiao, Z.H.; Xiong, S.B.; Li, C.H.; Liu, Y.; Yang, Z.D.; Feng, X.X.; Liu, X.W. Types of uranium deposits in central Zhuguang Mountains in Hunan Province, South China and their metallogenic regularity and prospecting directions. *Chin. Geol.* **2020**, *3*, 411–424.
6. Huang, H.Y.; Huang, S.D.; Chen, P.R. Analysis of geological setting of uranium mineralization in Jiuquling area, Hunan. *Uranium Geol.* **2006**, *22*, 276–280, (In Chinese with English Abstract).
7. Du, L.T.; Wang, W.G.; Liu, Z.Y. *Research and Evaluation of Uranium Deposits in China Volume I Granite-Related Uranium Deposits*, 1st ed.; Beijing Research Institute of Uranium Geology: Beijing, China, 2011; pp. 320–357. (In Chinese)
8. Ouyang, P.N.; Wang, Q.L. Analysis of uranium metallogenic conditions in Xiucaidong area, Rucheng County, Hunan Province. *Geol. Rev.* **2013**, *59*, 837–838. (In Chinese)
9. Lan, H.F.; Ling, H.F.; Chen, W.F.; Liu, J.W.; Ouyang, P.L. Analysis of rock genesis and uranium production potential of Sanjiangkou East rock mass. *Geol. J. Chin. Univ.* **2018**, *24*, 172–184, (In Chinese with English Abstract).
10. Lan, H.F. Study on Petrogenesis and Uranium Mineralization Potential of Sanjiu Area Granites in Southern Zhuguangshan Composite Pluton. Master’s Thesis, Nanjing University, Nanjing, China, 2015. (In Chinese with English Abstract).
11. Wang, Q.L.; Jiang, H.A.; Ouyang, P.L.; Zhang, Y. Analysis on geological feature of uranium mineralization and prospecting potential in Zhongshan area of middle Zhuguangshan. *Uranium Geol.* **2017**, *33*, 16–21, (In Chinese with English Abstract).
12. Wang, Q.L.; Li, K.; Qu, L.P. Ore-controlling factor and exploring direction of Jiuquling uranium deposit in “Sanjiu” region. *J. East Chin. Univ. Technol.* **2021**, *44*, 553–560, (In Chinese with English Abstract).
13. Chen, X.; Zhang, S.F. Study on the geological characteristics of uranium metallogenesis and the spatial distribution of uranium ore bodies in Jiulongjiang mining area in Sanjiu area. *Land Resour. Her.* **2016**, *13*, 9–13, (In Chinese with English Abstract).
14. Jiang, B.G.; He, Y.Y.; Chen, X.; Luo, W.Q.; Tan, Q.; Qin, J.N. Mineralization and metallogenic model of Sanjiangkou uranium deposit in “Sanjiu” area. *Uranium Geol.* **2017**, *33*, 266–272, (In Chinese with English Abstract).
15. Chen, X.; Liu, X.D.; Pan, J.Y.; Jiang, B.G.; Qin, J.N. Geochemical characteristics and geological significance of REE in Shibiwo occurrence located in south Jiulongjiang uranium deposit of Zhuguangshan massif. *J. Guil. Univ. Technol.* **2019**, *39*, 38–47, (In Chinese with English Abstract).
16. Feng, M.Y.; He, D.B. Uranium rich granite and uranium productive granite in south China. *Uranium Geol.* **2012**, *28*, 199–207, (In Chinese with English Abstract).
17. Zhao, K.D.; Jiang, S.Y.; Ling, H.F.; Sun, T.; Chen, W.F.; Chen, P.R.; Pu, W. Late Triassic U-bearing and barren granites in the Miao’ershan batholith, South China: Petrogenetic discrimination and exploration significance. *Ore Geol. Rev.* **2016**, *77*, 260–278. [[CrossRef](#)]
18. Zhai, Y.S. On the metallogenic system. *Earth. Sci. Front.* **1999**, *6*, 13–27, (In Chinese with English Abstract).
19. Zhao, Z.H. Microelement Geochemistry. *Adv. Earth. Sci.* **1992**, *7*, 65–66. (In Chinese)
20. Zhang, C.; Cai, Y.; Xu, H.; Dong, Q.; Liu, J.L.; Hao, R.X. Mechanism of mineralization in the Changjiang uranium ore field, South China: Evidence from fluid inclusions, hydrothermal alteration, and H–O isotopes. *Ore Geol. Rev.* **2017**, *86*, 225–253. [[CrossRef](#)]
21. Huang, H.Y.; Huang, S.D.; Cai, S.F. Analysis on geological setting of uranium mineralization and prospecting strategy in Lujing area, Hunan province. *World Nucl. Geosci.* **2008**, *25*, 63–67, (In Chinese with English Abstract).
22. Zhao, J.N.; Yu, Y.S. Application of trinity prospecting theory in analyzing metallogenic characteristics and metallogenic model of Chengkou deposit in Zhuguang integrated exploration area, northern Guangdong. *J. Geol.* **2018**, *42*, 283–290, (In Chinese with English Abstract).
23. Luo, Q.; Xu, Y.; Fu, S.C.; Guo, X.W. Uranium metallogenic geological characteristics and prospecting potential in Zhuguang Changjiang ore field. *Min. Expl.* **2020**, *11*, 276–285, (In Chinese with English Abstract).
24. Wang, Q.L.; Liu, X.Y.; Wang, T.; Jiang, H.A.; Xu, H.; Zhang, Y. Research on geochemical characteristics and uranium mineralization of Zhongpeng pluton in Zhongshan region of southern Hunan. *Uranium Geol.* **2017**, *33*, 273–279, (In Chinese with English Abstract).
25. Li, Y.; Xing, Y.Q.; Wang, S.M. *Methods for Chemical Analysis of Silicate Rocks*; Standards Press of China: Beijing, China, 2010; pp. 1–3. (In Chinese)
26. Li, C.H.; Chen, Y.; Han, B.Y. *Chemical Reagent-General Rules for Inductively Coupled Plasma Mass Spectrometry*; Standards Press of China: Beijing, China, 2020; pp. 1–17. (In Chinese)
27. Guo, S.; Ye, K.; Chen, Y.; Liu, J.B. A normalization solution to mass transfer illustration of multiple progressively altered samples using the isocon diagram. *Econ. Geol.* **2009**, *104*, 881–886. [[CrossRef](#)]

28. Wu, D.H.; Xia, F.; Pan, J.Y.; Liu, G.Q.; Huang, G.L.; Liu, W.Q.; Wu, J.Y. Characteristics of hydrothermal alteration and material migration of Mianhuakeng uranium deposit in northern Guangdong Province. *Acta Petrol. Sinica* **2019**, *35*, 2745–2764, (In Chinese with English Abstract).
29. Gresens, R.L. Composition-volume relationships of metasomatism. *Chem. Geol.* **1967**, *2*, 47–65. [[CrossRef](#)]
30. Grant, J.A. The isocon diagram; a simple solution to Gresens' equation for metasomatic alteration. *Econ. Geol.* **1986**, *81*, 1976–1982. [[CrossRef](#)]
31. Sun, S.S.; McDonough, W.F. Chemical and isotopic systematics of oceanic basalts: Implications for mantle compositions and processes. In *Magmatism in the Ocean Basins*, 1st ed.; Saunders, A.D., Norry, M.J., Eds.; Geological Society Special Publications: London, UK, 1989; Volume 42, pp. 313–345.
32. Chen, Z.Y.; Huang, G.L.; Zhu, B.; Chen, Z.H.; Huang, F.; Zhao, Z.; Tian, Z.J. The characteristics and metallogenic specialization of granite-hosted uranium deposits in the Nanling region. *Geotect. Metall.* **2014**, *38*, 264–275, (In Chinese with English Abstract).
33. Chen, Y.; Jin, R.S.; Miao, P.; Li, J.G.; Guo, H.; Chen, L.L. Occurrence of pyrites in sandstone-type uranium deposits: Relationships with uranium mineralization in the North Ordos Basin, China. *Ore Geol. Rev.* **2019**, *109*, 426–447. [[CrossRef](#)]
34. Zou, M.L.; Huang, H.Y.; Liu, X.Y.; Fan, L.T.; Xiang, T.F.; Xu, H.; Ouyang, P.L. Characterization of arsenic-bearing pyrite and the relationship with uranium metallogenic in the central Zhuguang pluton, Southern China. *Geol. Rev.* **2017**, *63*, 1021–1039, (In Chinese with English Abstract).
35. Cuney, M. Geologic environment, mineralogy, and fluid inclusions of the Bois Noirs–Limouzat uranium vein, Forez, France. *Econ. Geol.* **1978**, *73*, 1567–1610. [[CrossRef](#)]
36. Liu, T.G.; Zhao, Y.L.; Li, X.A. Preliminary Study of the relationship between irradiation damage and fluorite colour. *Acta Mineral. Sin.* **1983**, *4*, 300–304, (In Chinese with English Abstract).
37. Ryskin, A.I.; Fedorov, P.P.; Lushchik, A.; Generalov, M.E.; Angervaks, A.E.; Stolyarchuk, M.V.; Vasil'chenko, E.; Kudryavtseva, I. Absorption spectrum of dark purple fluorite, Kent deposit, Kazakhstan. *J. Fluor. Chem.* **2020**, *240*, 109654. [[CrossRef](#)]
38. Cheng, H.H.; Ma, H.F.; Xiang, W.D. Study on changes of existing state of uranium during alkalic metasomatism using fission-track method. *Uranium Geol.* **2000**, *16*, 291–296, (In Chinese with English Abstract).
39. Eggleton, R.A.; Banfield, J.F. The alteration of granitic biotite to chlorite. *Am. Mineral.* **1985**, *70*, 902–910.
40. Leroy, J. The Margnac and Fanay uranium deposits of the La Crouzille district (western Massif Central, France): Geologic and fluid inclusion studies. *Econ. Geol.* **1978**, *73*, 1611–1634. [[CrossRef](#)]
41. Ruzicka, V. Vein uranium deposits. *Ore Geol. Rev.* **1993**, *8*, 247–276. [[CrossRef](#)]
42. Wendlandt, R.F.; Harrison, W.J. Rare earth partitioning between immiscible carbonate and silicate liquids and CO₂ vapor: Results and implications for the formation of light rare earth-enriched rocks. *Contrib. Mineral. Petrol.* **1979**, *69*, 409–419. [[CrossRef](#)]
43. Michard, A.; Beaucaire, C.; Michard, G. Uranium and rare earth elements in CO₂-rich waters from Vals-les-Bains (France). *Geochim. Cosmochim. Acta* **1987**, *51*, 901–909. [[CrossRef](#)]
44. Ling, H.F. Origin of hydrothermal fluids of granite-type uranium deposits: Constraints from redox conditions. *Geol. Rev.* **2011**, *57*, 193–206, (In Chinese with English Abstract).
45. Hu, R.Z.; Bi, X.W.; Su, W.C.; Peng, J.T.; Li, C.Y. The relationship between uranium metallogenesis and crustal extension during the Cretaceous-Tertiary in South China. *Earth Sci. Front.* **2004**, *11*, 153–160, (In Chinese with English Abstract).
46. Chi, G.X.; Ashton, K.; Deng, T.; Xu, D.R.; Li, Z.H.; Song, H.; Liang, R.; Kennicott, J. Comparison of granite-related uranium deposits in the Beaverlodge district (Canada) and South China—A common control of mineralization by coupled shallow and deep-seated geologic processes in an extensional setting. *Ore Geol. Rev.* **2020**, *117*, 103319. [[CrossRef](#)]
47. Zhang, Y.Q.; Dong, S.W.; Li, J.H.; Li, J.H.; Cui, J.J.; Shi, W.; Su, J.B.; Li, Y. The new progress in the study of Mesozoic tectonics of South China. *Acta Geosci. Sin.* **2012**, *33*, 257–279, (In Chinese with English Abstract).
48. Guthrie, V.A.; Kleeman, J.D. Changing uranium distributions during weathering of granite. *Chem. Geol.* **1986**, *54*, 113–126. [[CrossRef](#)]
49. Chabiron, A.; Cuney, M.; Poty, B. Possible uranium sources for the largest uranium district associated with volcanism—The Streltsovka caldera (Transbaikalia Russia). *Miner. Depos.* **2003**, *38*, 127–140. [[CrossRef](#)]
50. Bonnetti, C.; Liu, X.D.; Mercadier, J.; Cuney, M.; Delouie, E.; Villeneuve, J.; Liu, W.Q. The genesis of granite-related hydrothermal uranium deposits in the Xiazhuang and Zhuguang ore fields, North Guangdong Province, SE China: Insights from mineralogical, trace elements and U-Pb isotopes signatures of the U mineralisation. *Ore Geol. Rev.* **2018**, *92*, 588–612. [[CrossRef](#)]
51. Min, M.Z.; Luo, X.Z.; Du, G.S.; He, B.A.; Campbell, A.R. Mineralogical and geochemical constraints on the genesis of the granite-hosted Huangao uranium deposit, SE China. *Ore Geol. Rev.* **1999**, *14*, 105–127. [[CrossRef](#)]
52. Min, M.Z.; Fang, C.Q.; Fayek, M. Petrography and genetic history of coffinite and uraninite from the Liueyiqi granite-hosted uranium deposit, SE China. *Ore Geol. Rev.* **2005**, *26*, 187–197. [[CrossRef](#)]
53. Göb, S.; Guhring, J.E.; Bau, M.; Markl, G. Remobilization of U and REE and the formation of secondary minerals in oxidized U deposits. *Am. Mineral.* **2013**, *98*, 530–548. [[CrossRef](#)]